ChemBioChem

Supporting Information

OsO_2 as the Contrast-Generating Chemical Species of Osmium-Stained Biological Tissues in Electron Microscopy

Ruiyu Li, Gregg Wildenberg, Kevin Boergens, Yingjie Yang, Kassandra Weber, Janek Rieger, Ashley Arcidiacono, Robert Klie, Narayanan Kasthuri,* and Sarah B. King*

SUPPORTING INFORMATION

Supporting Information

69451 Weinheim, Germany

OsO_2 as the contrast-generating chemical species of osmium-stained biological tissues in electron microscopy

Ruiyu Li, Gregg Wildenberg, Kevin Boergens, Yingjie Yang, Kassandra Weber, Janek Rieger, Ashley Arcidiacono, Robert Klie, Narayanan Kasthuri, and Sarah B. King*

Abstract: Electron imaging of biological samples stained with heavy metals has enabled visualization of nanoscale subcellular structures critical in chemical-, structural-, and neuro-biology. In particular, osmium tetroxide (OsO_4) has been widely adopted for selective lipid imaging. Despite the ubiquity of its use, the osmium speciation in lipid membranes and the process for contrast generation in electron microscopy (EM) have continued to be open questions, limiting efforts to improve staining protocols and therefore high-resolution nanoscale imaging of biological samples. Following our recent success using photoemission electron microscopy (PEEM) to image mouse brain tissues with synaptic resolution, we have used PEEM to determine the chemical contrast mechanism of Os staining in lipid membranes. Os(IV), in the form of OsO_2, generates nanoaggregates in lipid membranes, leading to a strong spatial variation in the electronic structure and electron density of states. OsO_2 has a metallic electronic structure that drastically increases the electron density of states near the Fermi level. Depositing metallic OsO_2 in lipid membranes allows for strongly enhanced EM signals and conductivity of biological materials. The identification of the chemical species and understanding of the membrane contrast mechanism of Os-stained biological specimens provides a new opportunity for the development of staining protocols for high-resolution, high-contrast EM imaging.

DOI: 10.1002/anie.2021XXXXX

SUPPORTING INFORMATION

Table of Contents

1. Experimental Procedures

1.1 Sample preparation for PEEM imaging

Mouse brain tissue processed in the Kasthuri lab was prepared as previously described[S1]. Briefly, mice were deeply anesthetized until unresponsive to pinch in limbs and tail. Mice were then transcardially perfused first with buffer (0.1 M sodium cacodylate, pH 7.4) followed by fixative (0.1 M sodium cacodylate, pH 7.4, 2% paraformaldehyde, and 2.5% glutaraldehyde). The brain was then extracted and incubated for 24 hours in fixative at 4 ◦C. Brains were vibratome sliced into 300 µm thick coronal sections. Next, a piece of cortical brain tissue ≈ 1 mm^2 was cut out with a scalpel, stained with heavy metals (i.e., osmium tetroxide, uranyl acetate, lead nitrate), dehydrated, and embedded in epoxy plastic. 40 nm ultrathin sections were cut on a Leica UC7 ultramicrotome using a Diatome Ultramaxi diamond knife and manually picked up on a 7 mm-by-7 mm silicon chip (with ≈ 2 nm native oxides) coated with 50 nm polycrystalline gold (AJA E-beam evaporator).

2. Results and Discussion

2.1 Energy-dependent PEEM imaging

Energy-dependent PEEM images were obtained by applying a high-pass energy filter to allow photoelectrons with kinetic energies higher than the threshold to be collected on the detector. As an example, **Figure S1**(a) is a representative PEEM image of an ultra-thin brain slice (UTBS) at energy filter $E\text{-}E_F$ = 2 eV, where E_F is the calibrated Fermi level of the analyzer, and $E\text{-}E_F$ is the work function difference between the sample and the ground that defines the absolute energy cut-off. For a selected ROI, as in the boxed region in **Figure S1**(a), intensity integrated over all pixels within the ROI can be plotted as a function of the energy filter as shown in **Figure S1**(b).

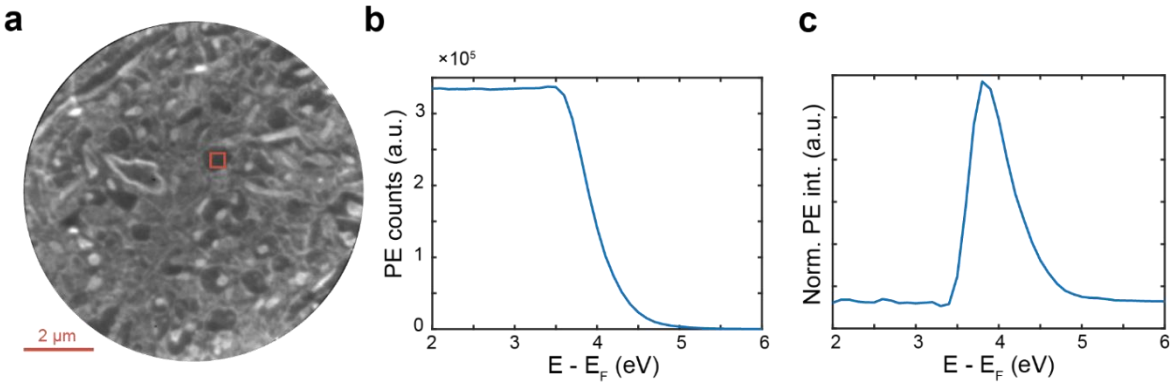

Figure S1 (a) A representative PEEM image of an ultra-thin brain slice (UTBS) at energy filter $E\text{-}E_F$= 2 eV. The red box indicates the ROI for integrating photoemission intensities. (b) Photoemission counts as a function of the high-pass energy filter. Intensities are integrated from all pixels within the boxed area in (a). (c) Difference spectrum of the sum photoemission counts from (b). The spectrum is normalized to the peak intensity.

The spectral information is extracted by subtracting subsequent high-pass energy-filtered images of total number N to obtain difference images Image diff(i) following the algorithm:

Image diff(1)=(Image(1)-Image(2))×2	for i = 1
Image diff(i)=Image(i-1)-Image(i+1)	for i = 2 to N-1
Image diff(N)=(Image(N-1)-Image(N))×2	for i = N

Figure S1(c) shows the photoemission spectrum of the ROI in **Figure S1**(a) after applying numerical differentiation, as the ones presented in the main text. This can then be utilized for comparing the work function difference from various regions of the specimen.

2.2 Fitting of photoemission spectra

The photoemission lineshape of secondary electrons can be reasonably described by an exponentially modified Gaussian function. The Gaussian distribution is written as:

$$G(x) = a_1 \frac{1}{\sqrt{2\pi}} e^{-\frac{(x-\mu)^2}{2\sigma^2}} \quad (1)$$

where a_1 is the amplitude, μ is the lateral offset, and σ is the standard deviation. And the exponential decay is:

$$E(x) = a_2 e^{-\lambda(x-\mu)} \quad (2)$$

where a_2 is the amplitude and λ is the rate of the decay. The functional form used to fit the photoemission spectrum is the convolution of the two functions, which takes of form of:

$$f(x) = G(x) * E(x) = a\, e^{\frac{\lambda^2\sigma^2}{2} - \lambda(x-\mu)}\, erfc\left[\frac{1}{\sqrt{2}}\left(\lambda\sigma - \frac{x-\lambda}{\sigma}\right)\right] + I_0 \quad (3)$$

where erfc is the complementary error function (erf) that is given by:

$$erfc(x) = 1 - \mathrm{erf}(x) = \frac{2}{\sqrt{\pi}} \int_x^{\infty} e^{-t^2}\, dt \quad (4)$$

Here, a is the amplitude of the photoemission intensity, and I0 is the intensity offset. μ represents the energy of the peak position. As shown in **Figure S2**, the difference spectrum obtained above, namely the photoemission spectrum, is fitted with Equation 3, where the secondary electron cutoff is calculated from the energy position that corresponds to half of the peak intensity. Here, the cutoff is found to be 3.63 eV, and the goodness of the fit is evaluated by the R^2, which is 0.997.

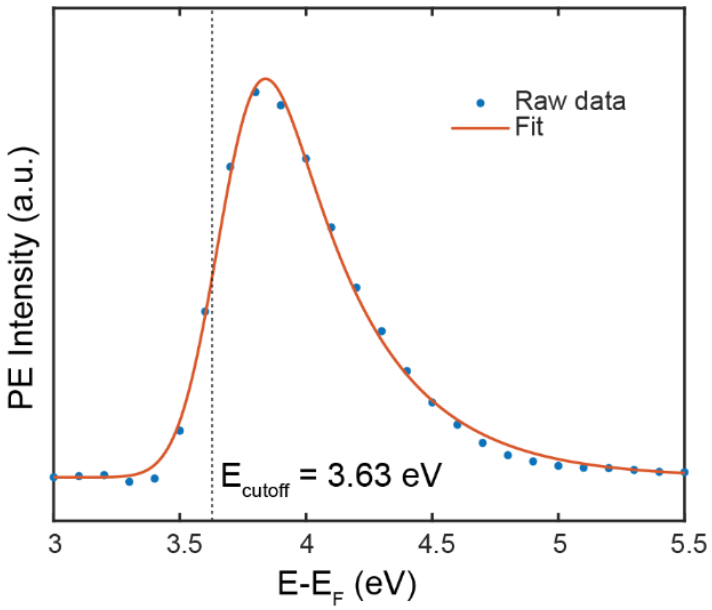

Figure S2 Photoemission spectrum fitted with exponentially-modified Gaussian function, showing the secondary electron cutoff at 3.63 eV.

2.3 STEM and EDS measurements

The UTBS were deposited on lacey carbon grids to improve electron conductivity, then imaged with a JEOL ARM200-CF equipped with a cold field-emission electron source, operated at 200 kV. Imaging and spectroscopic measurements were conducted with the emission current at 15 μA, an electron probe semi-convergence angle of 24 mrad, as well as inner and outer detector angles of 68 mrad and 280 mrad for high-angle annular dark-field (HAADF) imaging. To conduct nanoscale elemental identification and quantification, the JEOL ARM200CF is equipped with an Oxford XMAX100TLE X-ray windowless silicon drift detector (SDD) with a 100 mm^2 detector area. A full spectrum of the EDS measurements shown in Figure 3(c) in the main text is provided below (**Figure S3**).

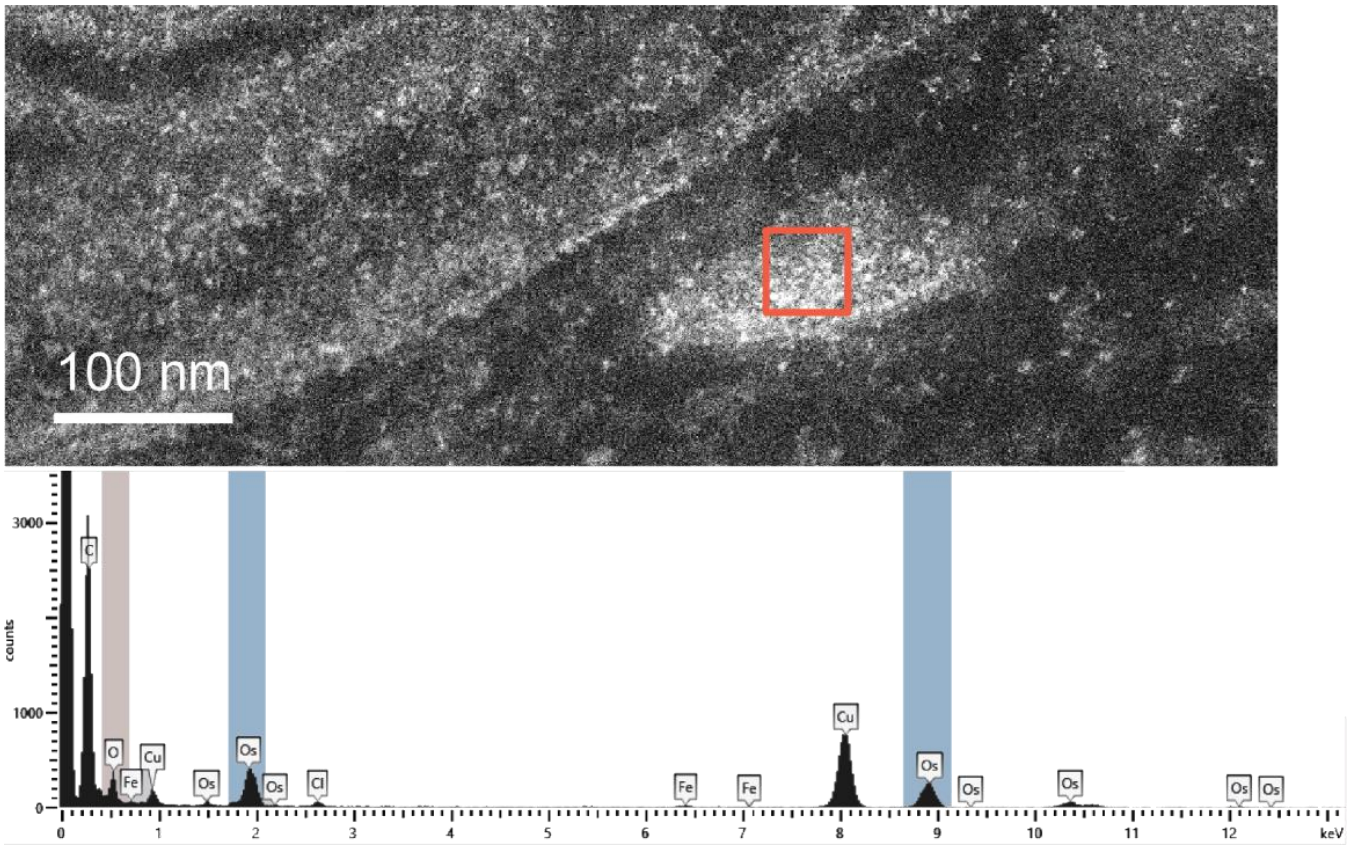

Figure S3 The full spectrum of the EDS measurements and the corresponding ROI.

2.4 EELS measurements

Electron energy-loss spectroscopy (EELS) measurements were conducted on Os-rich regions as well, using a post-columns Gatan Continuum GIF ER spectrometer, with an electron probe semi-convergence angle of 17.8 mrad and a collection angle of 53.4 mrad, as seen in Figure S3. A clear O edge and Os edge can be observed in the spectra. This corroborates the EDS results that Os is likely in an oxide form that also binds with the ligands around it, ruling out the possibility that Os exists as a majority of elemental Os. The low O concentrations detected by EDS rule out OsO_4 as the main chemical species. However, this does not rule out its existence entirely and there can still be a small amount of Os(VIII) in the sample. The combination of the EDS and EELS results indicates that Os most likely takes the valence state of IV, with some mixture of higher and lower states.

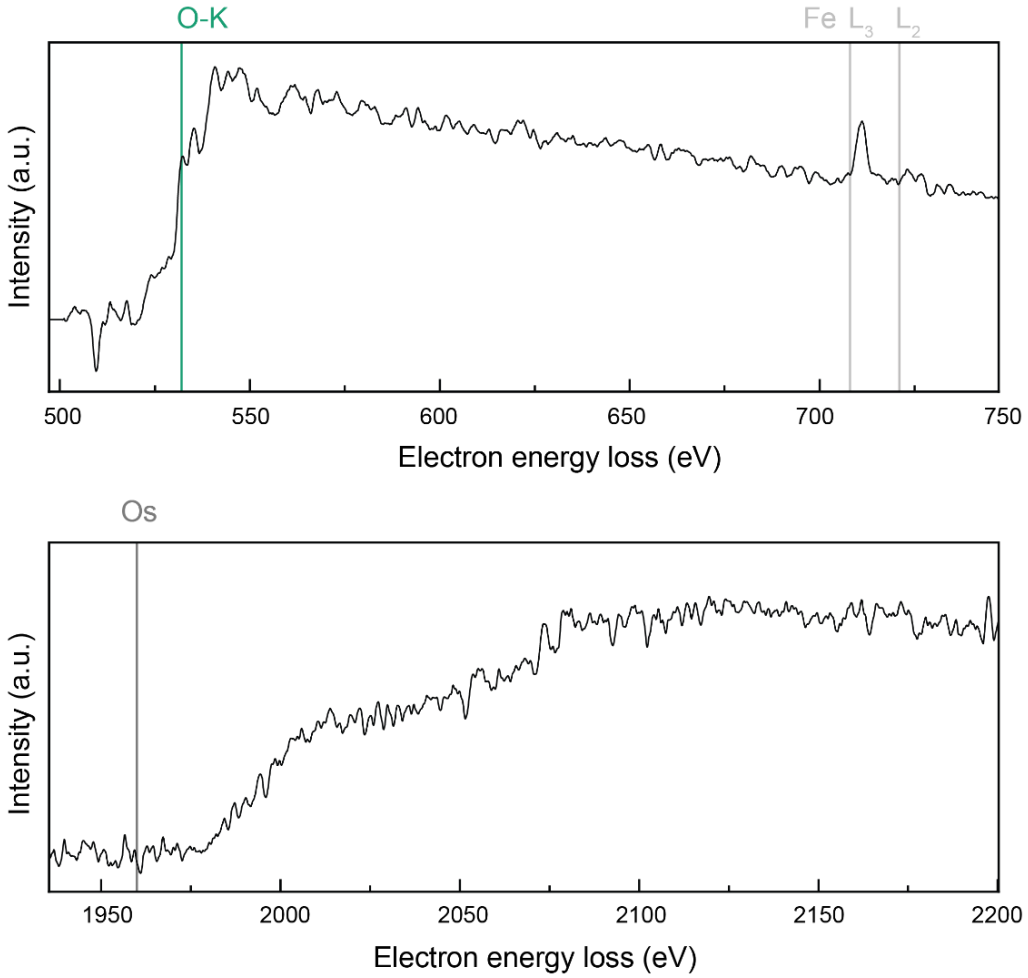

Figure S4 EELS spectra of two energy ranges, showing characteristic edges of oxygen (top spectrum) and osmium (bottom spectrum), respectively

3. Supplementary Figure(s)

3.1 Mercury lamp spectrum

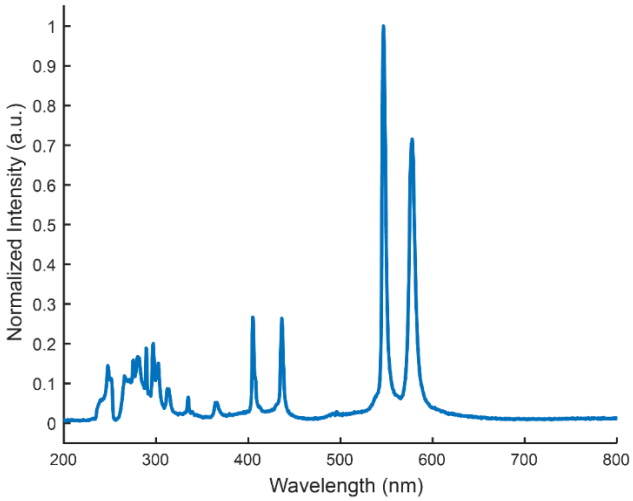

Figure S5 Optical spectrum of the Hg arc lamp, measured with an Ocean Insight Maya 2000 Pro spectrometer. Intensity is normalized to the highest peak.

3.2 Additional PEEM images of mouse brain tissues

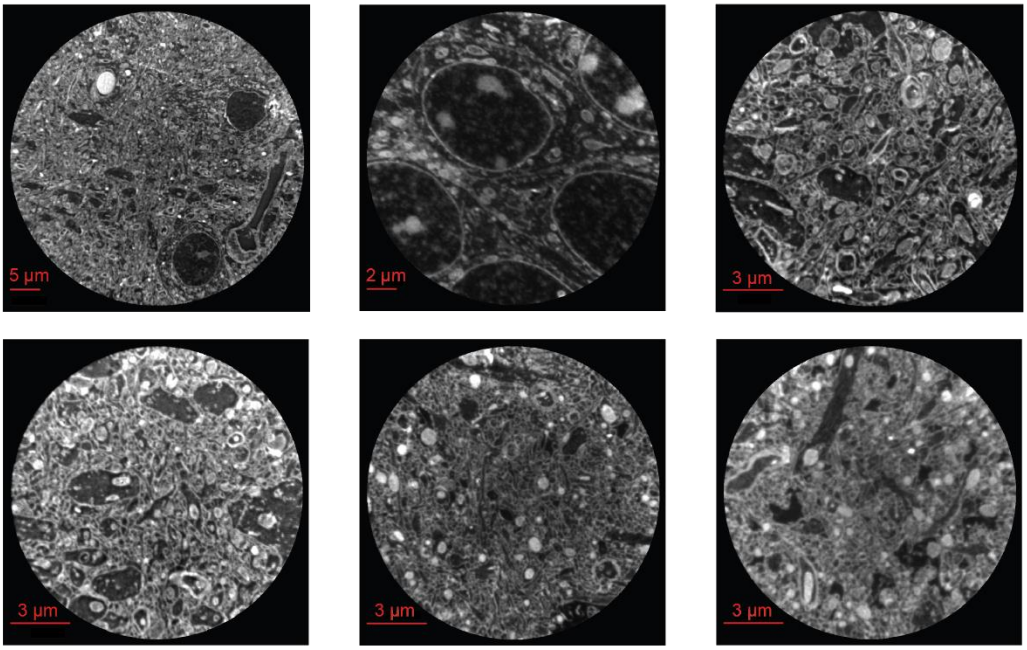

Figure S6 Additional PEEM images collected from different sets of mouse brain samples and at different dates, and with varying field of views. These images demonstrate the reproducibility of PEEM imaging method on Os-stained samples.

References

[S1] Y. Hua, P. Laserstein, M. Helmstaedter, *Nat. Commun.* **2015**, *6*, 7923.

Author Contributions

S.B.K., N.K. and R.K. designed the research. R.L., J.R., Y.Y. and K.W. performed the research. G.W. and K.B. contributed the samples. R.L., Y.Y., K.W. and A.A. analyzed the data. R.L. and A.A developed the chemical reaction model. R.L. and S.B.K. wrote the paper. S.B.K., R.K. and N.K. supervised the research.